Title
Digital Implementation of Adaptive Control Algorithms for MEMS Gyroscopes

Authors
Park, Sungsu
Horowitz, Roberto
Tan, Chin-woo

Publication Date
2002-03-01

CALIFORNIA PATH PROGRAM
INSTITUTE OF TRANSPORTATION STUDIES
UNIVERSITY OF CALIFORNIA, BERKELEY

Digital Implementation of Adaptive Control Algorithms for MEMS Gyroscopes

Sungsu Park, Roberto Horowitz, Chin-woo Tan
University of California, Berkeley

California PATH Research Report
UCB-ITS-PRR-2002-12

This work was performed as part of the California PATH Program of the University of California, in cooperation with the State of California Business, Transportation, and Housing Agency, Department of Transportation; and the United States Department of Transportation, Federal Highway Administration.

Report for MOU 329

March 2002

ISSN 1055-1425

Digital Implementation of Adaptive Control Algorithms for MEMS Gyroscopes

Sungsu Park
Roberto Horowitz

Department of Mechanical Engineering
University of California, Berkeley
{spark, horowitz}@newton.berkeley.edu

Chin-Woo Tan

California PATH
University of California, Berkeley
tan@robotics.eecs.berkeley.edu

MOU 329

Abstract

In this report, we present a hybrid discrete/ continuous time version of the observer-based adaptive control system for MEMS gyroscopes developed in [8], which can be readily implemented using digital processors. The control algorithm considered in this report is not fully a discrete time controller, since only the feedback control, parameter adaptation algorithms and feedforward control law are implemented in discrete time, while the velocity observer is still implemented in continuous time.
A stochastic analysis of this algorithm is developed and it shows that the estimates of the angular rate and the fabrication imperfections are biased due to the signal discretization errors in the feedforward control path introduced by the sampler and holder. Thus, a two-rate discrete time control is proposed as a compromise between the measurement biases due to discretization errors and the computational burden imposed on the controller due to a fast sampling rate. The convergence analysis of this algorithm is also conducted and an analysis method is developed for determining the trade-off between the controller sampling frequency and the magnitude of the angular rate estimate biased errors. All convergence and stochastic properties of a continuous time adaptive control are preserved, and this analysis is verified with computer simulations.

1. Introduction

Gyroscopes are commonly used sensors for measuring angular velocity in many areas of applications such as navigation, homing, and control stabilization. Although, conventional rotating wheel, fiber optic and ring laser gyroscopes have dominated a wide range of applications, they are too large and, most often too expensive to be used in most emerging applications.

Recent advances in micro-machining technology have made the design and fabrication of MEMS (Micro-Electro-Mechanical Systems) gyroscopes possible. These devices are several orders of magnitude smaller than conventional mechanical gyroscopes, and can be fabricated in large quantities by batch processes. Thus, there is great potential to significantly reduce their fabrication cost. The emergence of MEMS gyroscopes is opening up new market opportunities and applications in the area of low-cost to medium performance inertial devices [1].

Most MEMS gyroscopes are laminar vibratory mechanical structures fabricated on polysilicon or crystal silicon. Common fabrication steps include bulk micromachining, wafer-to-wafer bonding, surface micromachining, and high aspect ratio micromachining. Each of these fabrication steps involves multiple process steps such as deposition, etching and patterning of materials. Generally, every fabrication step contributes to imperfections in the gyroscope [2]. Fabrication imperfections that produce asymmetric structures, mis-alignment of actuation mechanism and deviations of the center of mass from the geometric center, result in undesirable, systematic perturbations in the form of mechanical and electrostatic forces, which degrade the performance of a gyroscope. Traditionally, manual mechanical or electrical balancing has been used to cancel parasitic effects with an open-loop mode of operation [3-5]. Although this procedure reduces the effect of a certain amount of imperfections, it is time consuming, expensive and difficult to perform on small, nail-size (*mm* level) gyroscopes. Two different types of controllers have been proposed for conventional closed-loop mode of operation in the literature. One is a Kalman filter based

preview control [6] and the other is a recently published force-balancing feedback control scheme using sigma-delta modulation [7]. Although these feedback control techniques increase the bandwidth and dynamic range of the gyroscope beyond the open-loop mode of operation, they still are sensitive to parameter variations such as damping, spring constant and quadrature error variations, produce ZRO and require tedious calibrations. The motion of a conventional mode-matched z-axis gyroscope does not have sufficient persistence of excitation, which makes it difficult to identify and compensate for all major fabrication imperfections in an on-line fashion. Moreover, some types of fabrication imperfections, which can be modeled as cross-damping terms, limit the minimum detectable angular rate signals.

Recently, a new gyroscope operation mode and a corresponding adaptive control algorithm have been developed, which are well suited for the on-line compensation of imperfects and to operate in varying environments that affect the behavior of a MEMS gyroscope [8]. This adaptive controlled gyroscope is self-calibrating, compensates for friction forces and fabrication imperfections that normally cause quadrature errors, and produces an unbiased angular velocity measurement that has no ZRO.

The adaptive control algorithm presented in [8] is a continuous time controller. It is assumed that the control and parameter adaptation laws are updated continuously in time. Although the implementation of such a controller is certainly possible utilizing analog circuits, it is of practical interest to explore the implementation of the adaptive control laws utilizing digital computers.

In this report, we present a hybrid discrete/continuous time version of the observer-based adaptive control system developed in [8], which can be readily implemented using digital processors. The control algorithm considered in this report is not fully a discrete time controller, since only the feedback control, parameter adaptation algorithms and feedforward control law are implemented in discrete time, while the velocity observer is still implemented in continuous time.

In the next section, the dynamics of MEMS gyroscopes is presented, by accounting for the effect of fabrication imperfections. In section 3, the observer-based adaptive control

algorithm presented in [8] is reviewed. The hybrid adaptive control law is developed in section 4. In section 5, the performance of the hybrid adaptive controlled gyroscope is analyzed, including magnitude of parameter estimation biases, convergence rate and resolution estimation. Finally, computer simulations are performed in section 6.

2. Dynamics of MEMS Gyroscopes

Common MEMS z-axis vibratory gyroscope configurations include a proof mass suspended by spring suspensions, and electrostatic actuations and sensing mechanisms for forcing an oscillatory motion and sensing the position and velocity of the proof mass. These mechanical components can be modeled as a two-degree-of-freedom mass, spring and damper system. To derive the gyroscope's dynamic equations of motion, two coordinate systems are introduced: the inertial frame, which is fixed in an inertial space, and the gyro frame, which is fixed to the rotation platform. Figure 1 shows a simplified model of a MEMS gyroscope having two degrees of freedom in the associated Cartesian reference frames.

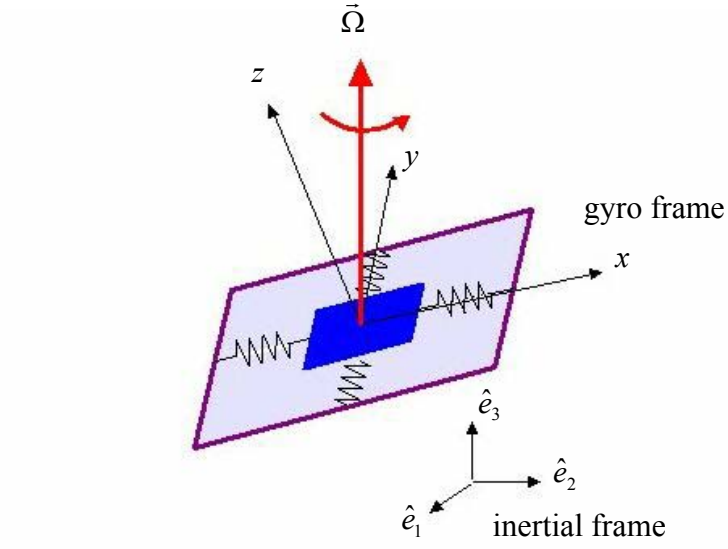

Figure 1. A model of a (planar vibratory) MEMS z-axis gyroscope

Assume that the gyro frame $\{g\}$ is rotated with respect to inertial frame $\{e\}$ by the angular velocity vector ${}^{e}\vec{\Omega}^{g}$, then the equation of the motion of the proof mass of the gyroscope is derived from Newton's law. If we wish to measure the component of the angular velocity along the *z*-axis, the motion of the proof mass can be constrained to be only along the *x*-*y* plane by making the spring stiffness in the *z* direction much larger than in the *x* and *y* directions. Assuming that the measured angular rate is almost constant over a long enough time interval and that linear accelerations are cancelled out, either as an offset from the output response or by applying counter-control forces, the equations of motion of a gyroscope are described in $\{g\}$ frame as follows.

$$\begin{aligned} m\ddot{x} + d_1\dot{x} + \left(k_1 - m(\Omega_y^2+\Omega_z^2)\right)x + m\Omega_x\Omega_y y &= \tau_x + 2m\Omega_z\dot{y} \\ m\ddot{y} + d_2\dot{y} + \left(k_2 - m(\Omega_x^2+\Omega_z^2)\right)y + m\Omega_x\Omega_y x &= \tau_x - 2m\Omega_z\dot{x} \end{aligned} \tag{1}$$

where *x* and *y* are the coordinates of the proof mass relative to the gyro frame, $d_{1,2}$, $k_{1,2}$ are damping and spring coefficients, $\Omega_{x,y,z}$ are the angular velocity components along each axis of the gyro frame and $\tau_{x,y}$ are control forces. In practice, small fabrication imperfections always occur, and cause dynamic coupling between the *x* and *y* axes through the asymmetric spring and damping terms.

Taking into account fabrication imperfections, the dynamic equation (1) is modified as follows [9].

$$\begin{aligned} m\ddot{x} + d_{xx}\dot{x} + d_{xy}\dot{y} + k_{xx}x + k_{xy}y &= \tau_x + 2m\Omega_z\dot{y} \\ m\ddot{y} + d_{xy}\dot{x} + d_{yy}\dot{y} + k_{xy}x + k_{yy}y &= \tau_y - 2m\Omega_z\dot{x} \end{aligned} \tag{2}$$

Equation (2) is the governing equation for a *z*-axis MEMS gyroscope. Fabrication imperfections contribute mainly to the asymmetric spring and damping terms, k_{xy} and d_{xy}. Therefore these terms are unknown, but can be assumed to be small. The *x* and *y* axes spring and damping terms are mostly known, but have small unknown variations from their

nominal values. The proof mass can be determined very accurately. However, even if there are small-unknown variations in the proof mass, this will not be a problem, because equation (2) can be scaled by the proof mass. The components of angular rate along *x* and *y* axes are absorbed as part of the spring terms as unknown variations. Note that the spring coefficients k_{xx} and k_{yy} include the electrostatic spring softness.

Non-dimensionalizing the equations of motion of a gyroscope is useful because the numerical simulation is easy, even under the existence of large two time-scales differences in gyroscope dynamics. One time scale is defined by the resonant natural frequency of the gyroscope, $\sqrt{k_{xx}/m}$, the other by the applied angular rate Ω_z. Nondimensionalization also produces a unified mathematical formulation for a large variety of gyroscope designs. In this report, controllers will be designed based on non-dimensional equations. The realization to a dimensional control for the specific gyroscope can be easily accomplished by multiplying the dimensionalizing parameters by the non-dimensional controller parameters. Based on m, q_0 and ω_n, which are a reference mass, length and natural resonance frequency respectively, where m is a proof mass of the gyroscope, the non-dimensionalized equation can be derived as follows:

$$\begin{aligned} \ddot{x} + \omega_x / Q_x \, \dot{x} + d_{xy}\dot{y} + \omega_x^2 x + \omega_{xy} y &= \tau_x + 2\Omega_z \dot{y} \\ \ddot{y} + d_{xy}\dot{x} + \omega_y / Q_y \, \dot{y} + \omega_{xy} x + \omega_y^2 y &= \tau_y - 2\Omega_z \dot{x} \end{aligned} \tag{3}$$

where Q_x and Q_y are respectively the *x* and *y* axis quality factor, $\omega_x = \sqrt{k_{xx}/(m\omega_0^2)}$, $\omega_y = \sqrt{k_{yy}/(m\omega_0^2)}$, $\omega_{xy} = k_{xy}/(m\omega_0^2)$, $d_{xy} \leftarrow d_{xy}/(m\omega_0)$, $\Omega_z \leftarrow \Omega_z/\omega_0$, $\tau_x \leftarrow \tau_x/(m\omega_0^2 q_0)$ and $\tau_y \leftarrow \tau_y/(m\omega_0^2 q_0)$. The natural frequency of the *x* or *y* axis can be used to define the nondimensionalizing parameter ω_0. Since the usual displacement range of the MEMS gyroscope in each axis is sub-micrometer level, it is reasonable to choose $1\,\mu$m as a reference length q_0.

3. Adaptive Mode of Operation

The aim of the adaptive mode of operation scheme presented in [8] is to achieve (1) on-line compensation of fabrication imperfections, (2) closed-loop identification of the angular rate, (3) to attain a large bandwidth and dynamic range, and (4) self-calibration operation. The adaptive mode of operation operates based on the observer-based adaptive control which needs only position measurements of the proof mass of the gyroscope.

For convenience, governing equation (3) of the MEMS gyroscopes is re-written as matrix form:

$$\ddot{q} + D\dot{q} + Kq = \tau - 2\Omega\,\dot{q} + b \tag{4}$$

where b is Brownian noise and

$$q = \begin{bmatrix} x \\ y \end{bmatrix} \quad \tau = \begin{bmatrix} \tau_x \\ \tau_y \end{bmatrix} \quad \Omega = \begin{bmatrix} 0 & -\Omega_z \\ \Omega_z & 0 \end{bmatrix}$$

$$D = \begin{bmatrix} d_{xx} & d_{xy} \\ d_{xy} & d_{yy} \end{bmatrix} \quad K = \begin{bmatrix} \omega_x^2 & \omega_{xy} \\ \omega_{xy} & \omega_y^2 \end{bmatrix}$$

The adaptive control problems of the gyroscope is formalized as follows: given equation (4) with unknown constant parameters D, K and Ω, determine the control law τ based on measuring q, such that the dynamic range is constrained within a specified region and Ω is estimated correctly.

Note that direct measurement of the velocity of the proof mass is avoided in the problem formulation. This is because current velocity sensing circuitry technology produces a noise with spectral power that is 3 to 4 orders of magnitude larger than the ideally expected value, as compared with position sensing technology.

The observer-based adaptive control and parameter adaptation laws are introduced in [8] as follows:

$$\tau = -\gamma(\dot{\hat{q}}_p^c - \dot{q}_m) + \hat{D}\dot{q}_m + \hat{R}q_m + 2\hat{\Omega}\dot{q}_m \tag{5}$$

$$\begin{aligned}
\dot{\hat{R}} &= \frac{1}{2}\gamma_R\left(\tau_0 q_m^T + q_m \tau_0^T\right) \\
\dot{\hat{D}} &= \frac{1}{2}\gamma_D\left(\tau_0 \dot{q}_m^T + \dot{q}_m \tau_0^T\right) \\
\dot{\hat{\Omega}} &= \gamma_\Omega\left(\tau_0 \dot{q}_m^T - \dot{q}_m \tau_0^T\right) \\
\tau_0 &= -(\dot{\hat{q}}_p^c - \dot{q}_m)
\end{aligned} \tag{6}$$

where $R = K - K_m$, $\hat{D}$, $\hat{R}$, $\hat{\Omega}$ are estimates of D, R and Ω, and $\gamma = diag\{\gamma_1, \gamma_2\}$, and γ_R, γ_D, and γ_Ω are adaptation gains.

Reference trajectory, $q_m = [x_m \;\; y_m]^T$, is updated by the following ideal oscillator,

$$\ddot{q}_m + K_m q_m = 0 \tag{7}$$

where $K_m = diag\{\omega_1^2, \omega_2^2\}$ are the reference resonant modes of both axis. Note that the signal q_m and $\dot{q}_m$ may be calculated and stored off-line, resulting in a significant reduction in the number of on-line computations.

The velocity estimate $\dot{\hat{q}}_p$ is corrupted by a measurement noise and produced by the following velocity observer.

$$\begin{aligned}
\dot{\hat{q}}_p^c &= \hat{q}_v^c + L(q + n - \hat{q}_p^c) \\
\dot{\hat{q}}_v^c &= -K_m \hat{q}_p^c
\end{aligned} \tag{8}$$

where n is a position measurement noise, which is assumed to be uncorrelated with Brownian noise b, and L is a observer gain matrix given by $L = diag\{L_1, L_2\}$. The estimated power spectral densities of the position measurement noise (S_p) and Brownian noise (S_b) measurements are given by [3,4]

$$S_p = \left(\frac{2C_0 + C_p}{2V_0 \dfrac{dC}{dy}} \right)^2 4k_B T R_{wire}, \; S_b = \frac{4k_B T d}{m} \tag{9}$$

where k_B, C_p, C_0, R_w, T, d and m are respectively Boltzmann's constant, the device's parasite capacitance, nominal sensing capacitance, wiring resistance, absolute temperature, damping coefficient and mass. Both are assumed zero-mean white noises.

We present the following two theorems without proof. The proofs can be found in [8].

Theorem 1 (Stability)

Given the observer (8), the adaptive control (5) and parameter adaptation laws (6), it is always possible to choose a velocity observer gain L, which makes the trajectory error, $e_p = q - q_m$, trajectory estimation errors, $\tilde{q}_p = \hat{q}_p - q$ and $\tilde{q}_v = \hat{q}_v - \dot{q}$, and their time derivatives converge locally, uniformly and exponentially to zero.

Theorem 2 (Persistent excitation condition)

With control law (5), parameter adaptation laws (6), and the observer (8), if the gyroscope is controlled to follow the mode-unmatched reference model, i.e. $\omega_1 \neq \omega_2$, the persistent excitation condition is satisfied and all unknown gyroscope parameters, including the angular rate, are estimated correctly.

Theorems 1 and 2 show that the motion of a mode-unmatched gyroscope, in which the resonance frequency of the x-axis is different from that of the y-axis, has sufficient

persistence of excitation to permit the identification of all major fabrication imperfections as well as "input" angular rate. This means that adaptive controlled gyroscope has no ZRO and is self-calibrating.

The main advantages of the adaptive mode of operation proposed in this report include self-calibration, large robustness to parameter variations, and no zero-rate output. Moreover, the adaptive controller design is also easy to implement in high Q systems. Thus, the noise properties associated with a high Q system can be fully utilized. Another advantage of the adaptive mode of operation is that it is easy to adjust the trade-off between bandwidth and resolution by simply adjusting the angular rate adaptation gain.

4. Hybrid Adaptive Control Law

4.1 Discrete Time Adaptive Control

We now consider the implementation of the adaptive control algorithm described by equations (5)-(6) utilizing a digital computer. As stated earlier, the parameter adaptation algorithm (6) and control law (5) will be implemented in discrete time, while the observer (8) will be implemented in continuous time. Thus, the adaptive algorithm can no longer be analyzed as a continuous time system, but rather as a hybrid system which includes both discrete time and continuous time algorithms.

For convenience, let us define an adaptation gain matrix Γ, a signal regressor $W(q_m, \dot{q}_m)$, and parameter estimation errors $\tilde{\theta} = \hat{\theta} - \theta$ as follows:

$$\Gamma = diag\left\{\gamma_R,\ \frac{1}{2}\gamma_R,\ \gamma_R,\ \gamma_D,\ \frac{1}{2}\gamma_D,\ \gamma_D,\ \frac{1}{2}\gamma_\Omega\right\}$$

$$W^T(q_m, \dot{q}_m) = \begin{bmatrix} x_m & y_m & 0 & \dot{x}_m & \dot{y}_m & 0 & -2\dot{y}_m \\ 0 & x_m & y_m & 0 & \dot{x}_m & \dot{y}_m & 2\dot{x}_m \end{bmatrix}$$

$$\theta^T = [r_{xx} \quad r_{xy} \quad r_{yy} \quad d_{xx} \quad d_{xy} \quad d_{yy} \quad \Omega_z]$$

where r_{ij}, d_{ij} and Ω_z are respectively elements of R, D and Ω.

Also, let us define the sampling index k and the sampling time Δt, such that $t_k = k\Delta t$. We define the hold operator H such that, $H[s(t_k)]$ denotes

$$H[s(t_k)] = \begin{cases} s(t_k) & \text{if } t_k \le t < t_{k+1} \\ s(t_{k+1}) & \text{if } t = t_{k+1} \end{cases} \tag{10}$$

Using $W_m(t)$ as a short hand notation for $W(q_m, \dot{q}_m)$, let us define $W_m(k)$ as

$$W_m(k) = W_m(t_k) = W(q_m(t_k), \dot{q}_m(t_k)) \tag{11}$$

Now, define the discrete time adaptive control law as

$$\tau(t) = -\gamma\, H[(\dot{\hat{q}}_p^c(k) - \dot{q}_m(k)) + \delta q(k)] + H[W_m^T(k)\hat{\theta}(k)] \tag{12}$$

where $\delta q(k)$ is a quantization noise of the velocity estimate. Because of finite word length error or digital computational error, the actual signal $W_m(k)$ must also be modeled as $W_a(k) = W_m(k) + \delta W_m(k)$, where $\delta W_m(k)$ is a finite word length error. However, since the signal $W_m(k)$ is known in advance and can be generated by the computer, its finite word length error can be made arbitrary small and will be neglected here. Note that the signal $W_m(k)$ may be calculated and stored in an off-line fashion, resulting in a significant reduction in the number of on-line computations.

The parameter estimate sequence $\hat{\theta}(k)$ in the equation (12) is updated by the following approximated continuous time parameter adaptation law.

$$\int_{t_k}^{t_{k+1}} \dot{\hat{\theta}}(t)\ dt = \int_{t_k}^{t_{k+1}} -\Gamma H\left[W_m(k)\gamma\ (\dot{\hat{q}}_p^c(k) - \dot{q}_m(k) + \delta q(k))\right] dt \tag{13}$$

Thus,

$$\hat{\theta}(k+1) = \hat{\theta}(k) - \Gamma W_m(k)\gamma\ [\dot{\hat{q}}_p^c(k) - \dot{q}_m(k) + \delta q(k)]\Delta t \tag{14}$$

or

$$\begin{aligned}
\hat{R}(k+1) &= \hat{R}(k) + \frac{1}{2}\Delta t\gamma_R\left(\tau_0(k)q_m^T(k) + q_m(k)\tau_0^T(k)\right) \\
\hat{D}(k+1) &= \hat{D}(k) + \frac{1}{2}\Delta t\gamma_D\left(\tau_0(k)\dot{q}_m^T(k) + \dot{q}_m(k)\tau_0^T(k)\right) \\
\hat{\Omega}(k+1) &= \hat{\Omega}(k) + \Delta t\gamma_\Omega\left(\tau_0(k)\dot{q}_m^T(k) - \dot{q}_m(k)\tau_0^T(k)\right) \\
\tau_0(k) &= -(\dot{\hat{q}}_p^c(k) - \dot{q}_m(k))
\end{aligned} \tag{15}$$

while the observer signals $\dot{\hat{q}}_p^c(t)$ and $\hat{q}_v^c(t)$ are still updated by the continuous time observer (8) and sampled at every Δt.

4.2 Stability Analysis

In order to derive the closed loop error equations, we apply the control law (12) and the adaptation algorithm (15) to the system equation (4) and observer (8). Define the signal discretization error function as

$$\Delta W_m(t) = H[W_m(k)] - W_m(t) \tag{16}$$

then the trajectory error equations are

$$\begin{aligned}
&\ddot{e}_p + (D + 2\Omega)\dot{e}_p + K_m e_p \\
&\quad = -\gamma\ H[\dot{e}_p(k) + \dot{\tilde{q}}_p(k) + \delta q(k)] + H[W_m^T(k)\hat{\theta}(k)] - W_m^T(t)\theta - \mathrm{Re}_p + b
\end{aligned} \tag{17}$$

where

$$H[W_m^T(k)\hat{\theta}(k)] - W_m^T(t)\theta = H[W_m^T(k)\tilde{\theta}(k)] + \left\{H[W_m^T(k)] - W_m^T(t)\right\}\theta$$
$$= H[W_m^T(k)\tilde{\theta}(k)] + \Delta W_m^T(t)\theta$$

The trajectory estimation error equations are

$$\begin{aligned}
\dot{\tilde{q}}_p &= \tilde{q}_v - L\tilde{q}_p + Ln \\
\dot{\tilde{q}}_v &= -K_m\tilde{q}_p + (D + 2\Omega)\dot{e}_p + \gamma\ H[\dot{e}_p(k) + \dot{\tilde{q}}_p(k) + \delta q(k)] \\
&\quad - H[W_m^T(k)\tilde{\theta}(k)] - \Delta W_m^T(t)\theta + \mathrm{Re}_p - b
\end{aligned} \tag{18}$$

where $e_p = q - q_m$, $\tilde{q}_p = \hat{q}_p^c - q$, and $\tilde{q}_v = \hat{q}_v^c - \dot{q}$. Equations (17) and (18) can be described compactly by the sum of a linear known and a linear unknown term as follows:

$$\begin{aligned}
\dot{\boldsymbol{x}}_c &= \boldsymbol{A}_c\boldsymbol{x}_c + \boldsymbol{A}_{cu}\boldsymbol{x}_c \\
&\quad - \boldsymbol{B}_c\gamma\ H[\dot{e}_p(k) + \tilde{q}_v(k) - L\tilde{q}_p(k) + Ln_s(k) + \delta q(k)] \\
&\quad + \boldsymbol{B}_c H[W_m^T(k)\tilde{\theta}(k)] + \boldsymbol{B}_c\Delta W_m^T(t)\theta + \boldsymbol{B}_c b + \boldsymbol{C}_c n
\end{aligned} \tag{19}$$

where $n_s(k)$ is the sampled measurement noise, where $n_s(k) \sim (0, S_p/\Delta t)$, $\boldsymbol{x}_c = \left[e_p\ \ \dot{e}_p\ \ \tilde{q}_p\ \ \tilde{q}_v\right]^T$ and

$$\boldsymbol{A}_c = \begin{bmatrix} 0 & I & 0 & 0 \\ -K_m & 0 & 0 & 0 \\ 0 & 0 & -L & I \\ 0 & 0 & -K_m & 0 \end{bmatrix}, \boldsymbol{B}_c = \begin{bmatrix} 0 \\ I \\ 0 \\ -I \end{bmatrix}, \boldsymbol{C}_c = \begin{bmatrix} 0 \\ 0 \\ L \\ 0 \end{bmatrix}, \boldsymbol{A}_{cu} = \begin{bmatrix} 0 & 0 & 0 & 0 \\ -R & -(D+2\Omega) & 0 & 0 \\ 0 & 0 & 0 & 0 \\ R & (D+2\Omega) & 0 & 0 \end{bmatrix}$$

Since the "control input" in equation (19),

$$H[\dot{e}_p(k) + \tilde{q}_v(k) - L\tilde{q}_p(k) + Ln_s(k) + \delta q(k)] + H[W_m(k)\tilde{\theta}(k)]$$

is held constant over the sampling period and the parameters are updated in a discrete time, it is convenient for the further analysis to discretize the trajectory and trajectory estimate error systems (17,18) as follows.

$$\begin{aligned}
\boldsymbol{x}_c(k+1) = {} & e^{(\boldsymbol{A}_c+\boldsymbol{A}_{cu})\Delta t}\boldsymbol{x}_c(k) \\
& - \int_{t_k}^{t_{k+1}} e^{(\boldsymbol{A}_c+\boldsymbol{A}_{cu})\ (t_k-t)}\boldsymbol{B}_c\gamma\ \ H[\dot{e}_p(k) + \tilde{q}_v(k) - L\tilde{q}_p(k) + Ln_s(k) + \delta q(k)]\ \ dt \\
& + \int_{t_k}^{t_{k+1}} e^{(\boldsymbol{A}_c+\boldsymbol{A}_{cu})\ (t_k-t)}\boldsymbol{B}_c H[W_m^T(k)\tilde{\theta}(k)]\ \ dt \\
& + \int_{t_k}^{t_{k+1}} e^{(\boldsymbol{A}_c+\boldsymbol{A}_{cu})\ (t_k-t)}\boldsymbol{B}_c\Delta W_m^T(t)\theta\ \ dt \\
& + \int_{t_k}^{t_{k+1}} e^{(\boldsymbol{A}_c+\boldsymbol{A}_{cu})\ (t_k-t)}\boldsymbol{B}_c b(t)\ \ dt \\
& + \int_{t_k}^{t_{k+1}} e^{(\boldsymbol{A}_c+\boldsymbol{A}_{cu})\ (t_k-t)}\boldsymbol{C}_c n(t)\ \ dt
\end{aligned} \tag{20}$$

If the sampling time is small, terms of order Δt^2 can be disregarded in a Taylor series expansion, and Euler's numerical approximation can be used to integrate equation (20). Thus,

$$\begin{aligned}
\boldsymbol{x}_c(k+1) \approx {} & (I + \boldsymbol{A}_c\Delta t)\boldsymbol{x}_c(k) + \boldsymbol{A}_{cu}\Delta t\ \ \boldsymbol{x}_c(k) \\
& - \boldsymbol{B}_c\Delta t\ \ \gamma\ \ [\dot{e}_p(k) + \tilde{q}_v(k) - L\tilde{q}_p(k) + Ln_s(k) + \delta q(k)] \\
& + \boldsymbol{B}_c\Delta t W_m^T(k)\tilde{\theta}(k) + \boldsymbol{C}(k)\theta + \boldsymbol{B}_c b_d(k) + \boldsymbol{C}_c n_d(k)
\end{aligned} \tag{21}$$

where

$$\boldsymbol{C}(k) = \int_{t_k}^{t_{k+1}} e^{(\boldsymbol{A}_c+\boldsymbol{A}_{cu})\ (t_k-t)}\boldsymbol{B}_c\Delta W_m^T(t)\ \ dt$$

and $b_d(k) \sim (0, S_b \Delta t)$, $n_d(k) \sim (0, S_p \Delta t)$. Notice that, in the numerical integration of equation (20) using Euler's approximation, the intensity of the sampled noises $b_d(k)$, $n_d(k)$ can be calculated by multiplying the intensity of noises $b(t)$, $n(t)$ by Δt . Utilizing the parameter adaptation law,

$$\begin{aligned}\widetilde{\theta}(k+1) &= \widetilde{\theta}(k) - \Delta t \Gamma W_m(k) \gamma \ [\dot{e}_p(k) + \dot{\widetilde{q}}_p(k) + \delta q(k)] \\ &= \widetilde{\theta}(k) - \Delta t \Gamma W_m(k) \gamma \, [\dot{e}_p(k) + \widetilde{q}_v(k) - L\widetilde{q}_p(k) + L n_s(k) + \delta q(k)]\end{aligned}$$

the extended error dynamics can be described by the following discrete time system.

$$\boldsymbol{x}_d(k+1) = \boldsymbol{A}_d(k)\boldsymbol{x}_d(k) + \boldsymbol{A}_{du}\boldsymbol{x}_d(k) + \boldsymbol{C}_d(k)\theta + \boldsymbol{G}_d \boldsymbol{w}_d(k) \tag{22}$$

where $\boldsymbol{x}_d = \begin{bmatrix} e_p & \dot{e}_p & \widetilde{q}_p & \widetilde{q}_v & \widetilde{\theta} \end{bmatrix}^T$, $\boldsymbol{w}_d = \begin{bmatrix} b_d & n_d & \delta q_d \end{bmatrix}^T$ and

$$\boldsymbol{A}_d(k) = \begin{bmatrix} I & \Delta t & 0 & 0 & 0 \\ -K_m \Delta t & I - \gamma \Delta t & \gamma L \Delta t & -\gamma \Delta t & W_m^T(k) \Delta t \\ 0 & 0 & I - L\Delta t & \Delta t & 0 \\ 0 & \gamma \Delta t & -(K_m + \gamma L)\Delta t & I + \gamma \Delta t & -W_m^T(k)\Delta t \\ 0 & -\Gamma W_m(k)\gamma \Delta t & \Gamma W_m(k) \gamma L \Delta t & -\Gamma W_m(k)\gamma \Delta t & I \end{bmatrix}$$

$$\boldsymbol{A}_{du} = \begin{bmatrix} 0 & 0 & 0 & 0 & 0 \\ -R\Delta t & -(D+2\Omega)\Delta t & 0 & 0 & 0 \\ 0 & 0 & 0 & 0 & 0 \\ R\Delta t & (D+2\Omega)\Delta t & 0 & 0 & 0 \\ 0 & 0 & 0 & 0 & 0 \end{bmatrix}, \ \boldsymbol{C}_d(k) = \begin{bmatrix} \boldsymbol{C}(k) \\ 0 \end{bmatrix}$$

$$\boldsymbol{G}_d = \begin{bmatrix} 0 & 0 & 0 \\ I & -\gamma L & -\gamma \\ 0 & L & 0 \\ -I & \gamma L & \gamma \\ 0 & -\Gamma W_m(k)\gamma L & -\Gamma W_m(k)\gamma \end{bmatrix}, \boldsymbol{w}_d(k) \sim (0, \boldsymbol{S}_d)$$

where $\boldsymbol{S}_d = diag(\boldsymbol{S}_c \Delta t,\ S_{quan}\Delta t^2)$, $\boldsymbol{S}_c = diag\{S_b, S_p\}$ and S_{quan} is the power spectral density of the quantization noise for δq. In order to prove the stability of the closed-loop system, we consider the stochastic expectation propagation of equation (22). Since the propagation equation has the same form as its deterministic counterpart, we can consider the deterministic case, i.e. $\boldsymbol{w}_d(k) = 0$. Since $\boldsymbol{A}_d(k)$ in equation (22) is a periodic discrete time-varying matrix with period $k_T = \dfrac{4\pi^2}{\omega_1 \omega_2 \Delta t}$, where ω_1 and ω_2 are the model reference frequencies, we can utilize a similar analytical procedure to be the one that was employed in [8] to analyze the stability of the continuous time varying error dynamics. To do that, we consider a discrete time version of Floquet theory.

Lemma (Discrete-Time Floquet theory)

Consider the following discrete time periodic time-varying linear system with period k_T,

$$x(k+1) = A(k)x(k), \text{ where } A(k) = A(k + k_T) \tag{23}$$

where $A(k)$ is a nonsingular matrix. Then, there exists a periodic transformation which converts the periodic time-varying linear system to a time invariant linear system.

Proof:

Let $\Phi(k)$ be a state transition matrix of the time varying linear system (23), Then

$$\Phi(k+1) = A(k)\Phi(k)$$

Consider

$$\begin{aligned} \Phi(k+1+k_T) &= A(k+k_T)\Phi(k+k_T) \\ &= A(k)\Phi(k+k_T) \end{aligned}$$

Thus, there exists a nonsingular constant matrix Q such that

$$\Phi(k+1) = \Phi(k)Q$$

Now, set $Q = \overline{A}^{k_T}$ and define $F(k) = \Phi(k)\overline{A}^{-k}$, then

$$\begin{aligned} F(k+k_T) &= \Phi(k+k_T)\overline{A}^{-k_T}\overline{A}^{-k} = \Phi(k)\overline{A}^{k_T}\overline{A}^{-k_T}\overline{A}^{-k} = \Phi(k)\overline{A}^{-k} \\ &= F(k) \end{aligned}$$

Therefore, the matrix $F(k)$ is a periodic matrix with the same period as the system, and can be considered as a state transformation matrix. Thus, consider the new state $z(k)$ such that $x(k) = F(k)z(k)$. If we substitute it into the system (23),

$$F(k+1)z(k+1) = A(k)F(k)z(k)$$

Thus,

$$z(k+1) = F^{-1}(k+1)A(k)F(k)z(k)$$

where

$$\begin{aligned} F^{-1}(k+1)A(k)F(k) &= \overline{A}\overline{A}^{k}\Phi^{-1}(k+1)A(k)\Phi(k)\overline{A}^{-k} \\ &= \overline{A}\overline{A}^{k}\Phi^{-1}(k)A^{-1}(k)A(k)\Phi(k)\overline{A}^{-k} \\ &= \overline{A} \end{aligned}$$

Finally, we get the state equation for the equivalent time invariant system:

$$z(k+1) = \overline{A}z(k)$$

and the lemma is proved.

Now, we are ready to prove the stability of the error dynamics of equation (22).

Theorem 3 (Stability)

Consider the adaptive control law and adaptation laws, given by equations (12) and (13), and the adaptive observer (8), which result in the error dynamics (22). If the sampling time Δt is sufficiently small, it is always possible to choose an observer gain L which will result in all error signals, $e, \dot{e}, \tilde{q}_p, \tilde{q}_v$ and $\tilde{\theta}$ being bounded. These bounds are a function of the discretization error introduced by sampling and the zero-order hold.

Proof:

Let $\Phi(k)$ be a state transition matrix associated with the periodic matrix $\boldsymbol{A}_d(k)$ in equation (22), i.e.

$$\Phi_d(k+1) = \boldsymbol{A}_d(k)\Phi_d(k) \tag{24}$$

then according to Lemma, the state transition matrix can be written as a product of two matrices as

$$\Phi_d(k) = \boldsymbol{F}_d(k)\overline{\boldsymbol{A}}_d^k$$

where $\boldsymbol{F}_d(k)$ is a discrete periodic nonsingular matrix with period k_T which satisfies condition, $\boldsymbol{F}_d(0) = \boldsymbol{F}_d(k_T) = I$. $\overline{\boldsymbol{A}}_d$ is a constant matrix and the stability of the linear time varying known dynamics

$$\boldsymbol{x}_{dn}(k+1) = \boldsymbol{A}_d(k)\boldsymbol{x}_{dn}(k) \tag{25}$$

is determined by eigenvalues of $\overline{\boldsymbol{A}}_d$. Similarly to the continuous time case, an appropriate observer gain L always exists such that the matrix $\overline{\boldsymbol{A}}_d$ will be stable, if the sampling time is made sufficiently small. In order to determine $\boldsymbol{F}_d(k)$, the state transition matrix $\Phi_d(k)$ must be computed. Unfortunately, it is hard to analytically compute $\Phi_d(k)$. Instead, the

transition matrix at the end of one period is numerically computed from equation (24) utilizing the initial condition $\Phi_d(0) = I$ and $\overline{\boldsymbol{A}}_d$ is obtained from $\overline{\boldsymbol{A}}_d = \Phi^{-k_T}(k_T)$.

The remainder of the stability proof is based on the Lyapunov function approach. Consider the following Lyapunov function candidate:

$$V(k) = \boldsymbol{x}_d^T(k)\boldsymbol{F}_d^{-T}(k)\boldsymbol{M}\boldsymbol{F}_d^{-1}(k)\boldsymbol{x}_d(k)$$

where $\boldsymbol{M}$ is the solution of Lyapunov function, $\overline{\boldsymbol{A}}_d^T\boldsymbol{M}\overline{\boldsymbol{A}}_d - \boldsymbol{M} = -\boldsymbol{I}$. Since $\overline{\boldsymbol{A}}_d$ is asymptotically stable, $\boldsymbol{M} > 0$ and $\boldsymbol{F}_d^{-T}(k)\boldsymbol{M}\boldsymbol{F}_d^{-1}(k) > 0$ for all $k \geq 0$. Using the following relationships, $\overline{\boldsymbol{A}}_d = \boldsymbol{F}_d^{-1}(k+1)\boldsymbol{A}_d(k)\boldsymbol{F}_d(k)$, and calculating the difference of V along the trajectory (22) gives

$$\begin{aligned}
\Delta V(k) &= V(k+1) - V(k) \\
&= \boldsymbol{x}_d^T(k+1)\boldsymbol{F}_d^{-T}(k+1)\boldsymbol{M}\boldsymbol{F}_d^{-1}(k+1)\boldsymbol{x}_d(k+1) \\
&\quad - \boldsymbol{x}_d^T(k)\boldsymbol{F}_d^{-T}(k)\boldsymbol{M}\boldsymbol{F}_d^{-1}(k)\boldsymbol{x}_d(k) \\
&= -\boldsymbol{x}_d^T(k)\boldsymbol{F}_d^{-T}(k)\boldsymbol{F}_d^{-1}(k)\boldsymbol{x}_d(k) \\
&\quad + \boldsymbol{x}_d^T(k)\boldsymbol{A}_{du}^T\boldsymbol{F}_d^{-T}(k+1)\boldsymbol{M}\boldsymbol{F}_d^{-1}(k+1)\boldsymbol{A}_{du}\boldsymbol{x}_d(k) \\
&\quad + 2\boldsymbol{x}_d^T(k)\boldsymbol{F}_d^{-T}(k)\overline{\boldsymbol{A}}_d^T\boldsymbol{M}\boldsymbol{F}_d^{-1}(k+1)\boldsymbol{A}_{du}\boldsymbol{x}_d(k) \\
&\quad + \theta^T\boldsymbol{C}_d^T(k)\boldsymbol{F}_d^{-T}(k+1)\boldsymbol{M}\boldsymbol{F}_d^{-1}(k+1)\boldsymbol{C}_d(k)\theta \\
&\quad + 2\boldsymbol{x}_d^T(k)\boldsymbol{F}_d^{-T}(k)\overline{\boldsymbol{A}}_d^T\boldsymbol{M}\boldsymbol{F}_d^{-1}(k+1)\boldsymbol{C}_d(k)\theta \\
&\quad + 2\boldsymbol{x}_d^T(k)\boldsymbol{A}_{du}^T\boldsymbol{F}_d^{-T}(k+1)\boldsymbol{M}\boldsymbol{F}_d^{-1}(k+1)\boldsymbol{C}_d(k)\theta
\end{aligned}$$

Since $\boldsymbol{F}(k)$ is a nonsingular matrix for all $k \geq 0$, $\boldsymbol{F}^{-T}(k)\boldsymbol{F}^{-1}(k) > 0$ for all $k \geq 0$. Thus,

$$\begin{aligned}
\Delta V(k) \leq\ & -\alpha_{\min}^2\|\boldsymbol{x}_d\|^2 + \alpha_{\max}^2\beta^2\lambda_{\max}(\boldsymbol{M})\|\boldsymbol{x}_d\|^2 + 2\alpha_{\max}^2\varepsilon\beta\lambda_{\max}(\boldsymbol{M})\|\boldsymbol{x}_d\|^2 \\
& + \alpha_{\max}^2\eta^2\lambda_{\max}(\boldsymbol{M})\|\theta\|^2 + 2\alpha_{\max}^2\eta\varepsilon\lambda_{\max}(\boldsymbol{M})\|\boldsymbol{x}_d\|\cdot\|\theta\| + 2\alpha_{\max}^2\beta\eta\lambda_{\max}(\boldsymbol{M})\|\boldsymbol{x}_d\|\cdot\|\theta\|
\end{aligned}$$

where $\alpha_{\min} = \min_{0\le k\le k_T} \left\| \boldsymbol{F}_d^{-1}(k) \right\|$, $\alpha_{\max} = \max_{0\le k\le k_T} \left\| \boldsymbol{F}_d^{-1}(k) \right\|$, $\eta = \max_{0\le k\le k_T} \left\| \boldsymbol{C}_d(k) \right\|$, $\beta = \left\| \boldsymbol{A}_{du} \right\|$ and $\varepsilon = \left\| \overline{\boldsymbol{A}}_d \right\|$. If the signal discretization error $\Delta W_m(t) = H[W_m(k)] - W_m(t)$ is zero, or equally $\eta = 0$, the origin of the state space $(e_p, \dot{e}_p, \tilde{q}_p, \tilde{q}_v, \tilde{\theta}) = 0$ is guaranteed to be locally uniformly exponentially stable within the domain of $\alpha_{\min}^2 > \alpha_{\max}^2 \lambda_{\max}(\boldsymbol{M})\beta(\beta + 2\varepsilon)$. Since some amount of discretization error is always present, the trajectory, trajectory estimation and parameter estimation errors will not converge to zero, but rather to a compact residual set. This residual set is defined by

$$\aleph = \left\{ \boldsymbol{x}_d : \left\| \boldsymbol{x}_d \right\| \le \eta \left\| \theta \right\| \cdot \left(\frac{b + \sqrt{b^2 + ac}}{a} \right) \right\}$$

where

$$a = \alpha_{\min}^2 - \alpha_{\max}^2 \lambda_{\max}(\boldsymbol{M})\beta(\beta + 2\varepsilon)$$

$$b = \alpha_{\max}^2 \lambda_{\max}(\boldsymbol{M})(\beta + \varepsilon),\ c = \alpha_{\max}^2 \lambda_{\max}(\boldsymbol{M})$$

and the theorem is proved.

5. Performance Analysis

5.1 Magnitude of Parameter Estimation Biases

As discussed in the stability analysis, the introduction of the signal discretization error function $\Delta W_m(t)$, which was defined in equation (16), prevents the error dynamics from asymptotically converging to zero and introduces bias in the estimates of the angular rate and fabrication imperfections. In order to reduce bias of the estimates, it is necessary to make this discretization error small by achieving a fast computation rate in the feedforward

control path. To choose an appropriate computation rate in the feedforward control path, it is necessary to determine the relationship between the computation rate and the magnitude of the bias estimate. Consider the signal discretization error term $\boldsymbol{C}(k)\theta$ in equation (21) and its average power. If its power is equal to the power spectral density of a fictitious noise term $\boldsymbol{G}_c\boldsymbol{w}(k)$, where

$$\boldsymbol{G}_c = \begin{bmatrix} 0 & 0 \\ I & -\gamma L \\ 0 & L \\ -I & \gamma L \end{bmatrix},\ \boldsymbol{w} = \begin{bmatrix} b_d \\ n_d \end{bmatrix} \sim (0, \boldsymbol{S}_c \Delta t)$$

where $\boldsymbol{S}_c = diag\{S_b, S_p\}$,the effect of the signal discretization error on the error dynamics of $e_p, \dot{e}_p, \tilde{q}_p, \tilde{q}_v$ and $\tilde{\theta}$ will be same to that of the noise in the stochastic average sense. Thus,

$$AVG\left(\boldsymbol{C}(k)\theta\theta^T\boldsymbol{C}(k)^T\right) = \boldsymbol{G}_c\boldsymbol{S}_c\boldsymbol{G}_c^T\Delta t \tag{26}$$

Equation (26) can be used to determine the following bound,

$$\max\left\|\boldsymbol{C}(k)\theta\right\|^2 = \left\|\boldsymbol{G}_c\right\|^2\left\|\boldsymbol{S}_c\right\|\Delta t \tag{27}$$

Using Euler's numerical integration approximation, $\left\|\boldsymbol{C}(k)\theta\right\|$ can be further approximated as follows.

$$\left\|\boldsymbol{C}(k)\theta\right\| \le \int_{t_k}^{t_{k+1}} \left\| e^{(\boldsymbol{A}_c+\boldsymbol{A}_{cu})\ (t_k-t)}\boldsymbol{B}_c\Delta W_m^T(t)\theta \right\|\ dt \le \left\|\boldsymbol{B}_c\right\|\ \left\|\Delta W_m^T(t)\theta\right\|_{\max}\Delta t$$

The right hand side of the above equation can be further expanded as follows.

$$\begin{aligned}\left\|\Delta W_m^T(t)\theta\right\| &= \left\|(D+2\Omega)\Delta\dot{q}_m(t)+R\Delta q_m(t)\right\| \\ &\le \max\left\{\left\|\Delta\dot{q}_m(t)\right\|\ \left\|D+2\Omega\right\|,\ \left\|\Delta q_m(t)\right\|\ \left\|R\right\|\right\} \\ &= \Delta t\max\left\{\sqrt{X_0^2\omega_1^4+Y_0^2\omega_2^4}\left\|D+2\Omega\right\|,\ \sqrt{X_0^2\omega_1^2+Y_0^2\omega_2^2}\left\|R\right\|\right\}\end{aligned}$$

Under the decoupling condition of the angular estimate and fabrication imperfection estimates [8], i.e. $X_0\omega_1 = Y_0\omega_2$, equation (27) becomes,

$$2\Delta t^2 X_0\omega_1\ \max\left(\omega_1\left\|D+2\Omega\right\|,\ \left\|R\right\|\right) = \left\|\boldsymbol{G}_c\right\|\sqrt{\Delta t\left\|\boldsymbol{S}_c\right\|} \tag{28}$$

Therefore, the required sampling time to achieve parameter estimation bias magnitude below or equal to the Brownian and position measurement noise floor is given by

$$\Delta t = \left(\frac{\left\|\boldsymbol{G}_c\right\|\sqrt{\left\|\boldsymbol{S}_c\right\|}}{2X_0\omega_1\ \max\left(\omega_1\left\|D+2\Omega\right\|,\ \left\|R\right\|\right)}\right)^{\frac{2}{3}} \tag{29}$$

where D is the damping matrix, R is the resonant frequency modeling error matrix, and Ω is the unknown "input" angular rate.

Equation (29) is a useful criterion for choosing an approximate computation rate for the feedforward control path. Equation (29) suggests that the magnitude of biases of the angular rate and fabrication imperfection estimates is proportional to the computation rate elevated to the $3/2$ as shown in Figure 2. However, it is important to note that "magnitude" in this context means the norm of a vector composed of the angular rate and fabrication imperfection estimate errors. Thus, individual biases such as the angular rate estimation bias, may be equal to or less than this estimate.

When the sampling rate of the discrete time control algorithm in equations (12) and (15) is increased significantly, the computational burden of the control algorithm may become too high, and may cause unnecessarily over-sampling in the parameter adaptation algorithm.

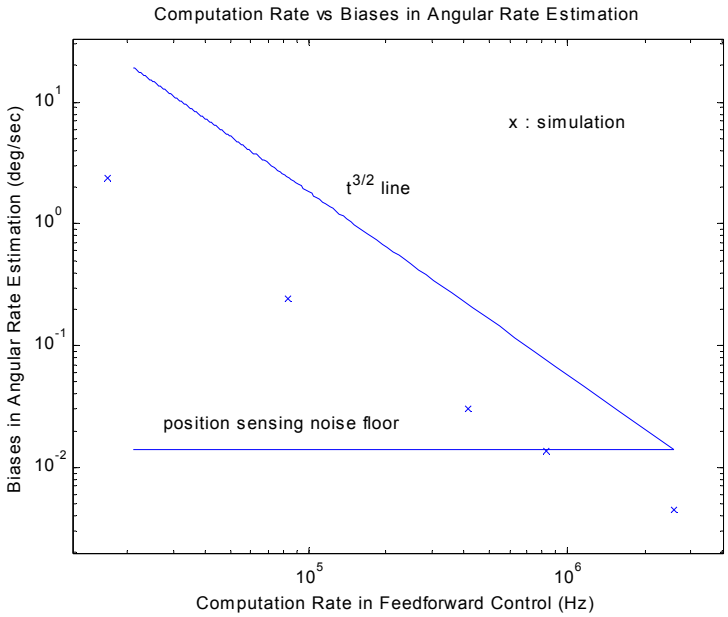

Figure 2. Computation rate in the feed forward control path vs bias in the parameter estimations

The sampling rate of the parameter adaptation algorithm may not be to be larger than two or three times the Nyquist frequency. This analysis suggests the introduction of a two-rate discrete time control as a compromise between minimizing bias estimate due to discretization errors and attaining an implemental controller computational burden. In this two-rate discrete time controller, the parameter adaptation algorithm is updated at a slower rate than the reference signal which is used in the feedforward control. The two-rate discrete time control is realized as follows:

$$\tau(t) = -\gamma \; H[(\hat{\dot{q}}_p(k) - \dot{q}_m(k))] + H[\hat{D}(k_f)\dot{q}_m(k_f) + \hat{R}(k_f)q_m(k_f) + 2\hat{\Omega}(k_f)\dot{q}_m(k_f)]$$

$$
\begin{aligned}
\hat{R}(k+1) &= \hat{R}(k) + \frac{1}{2}\Delta t\gamma_R\left(\tau_0(k)q_m^T(k) + q_m(k)\tau_0^T(k)\right) \\
\hat{D}(k+1) &= \hat{D}(k) + \frac{1}{2}\Delta t\gamma_D\left(\tau_0(k)\dot{q}_m^T(k) + \dot{q}_m(k)\tau_0^T(k)\right) \\
\hat{\Omega}(k+1) &= \hat{\Omega}(k) + \Delta t\gamma_\Omega\left(\tau_0(k)\dot{q}_m^T(k) - \dot{q}_m(k)\tau_0^T(k)\right) \\
\tau_0(k) &= -(\hat{\dot{q}}_p(k) - \dot{q}_m(k))
\end{aligned}
\tag{30}
$$

where H is the sample and hold operation defined in equation (10), $k = rk_f$ (or alternatively $\Delta t = r\Delta t_f$) where r is some integer greater than 1, and

$$
\begin{aligned}
\hat{D}(k_f + pk_f) &= \hat{D}(k) \\
\hat{R}(k_f + pk_f) &= \hat{R}(k) \\
\hat{\Omega}(k_f + pk_f) &= \hat{\Omega}(k)
\end{aligned}
$$

for $p = 1,...,r-1$.

5.2 Convergent Rate Analysis

In order to apply averaging analysis, consider the error dynamics given by equations (14) and (19). We will ignore the signal discretization error in the feedforward control path which causes the bias of the states. As in the continuous time counter part, we first assume that all noise terms are zero. If we do a state coordinate transformation from $\boldsymbol{x}_c = [e_p\ \dot{e}_p\ \tilde{q}_p\ \tilde{q}_v]^T$ to $\boldsymbol{x}_a = [e_p\ \dot{e}_p\ \tilde{q}_p\ \dot{\tilde{q}}_p]^T$, then

$$
\begin{aligned}
\dot{\boldsymbol{x}}_a &= \boldsymbol{A}_a\boldsymbol{x}_a + \boldsymbol{A}_{cu}\boldsymbol{x}_a \\
&\quad - \boldsymbol{B}_c\gamma\ H[\dot{e}_p(k) + \ddot{\tilde{q}}_p(k)] + \boldsymbol{B}_c H[W_m^T(k)\tilde{\theta}(k)] \\
\tilde{\theta}(k+1) &= \tilde{\theta}(k) - \Delta t\Gamma W_m(k)\gamma\ [\dot{e}_p(k) + \ddot{\tilde{q}}_p(k)]
\end{aligned}
\tag{31}
$$

where

$$\boldsymbol{A}_a = \begin{bmatrix} 0 & I & 0 & 0 \\ -K_m & 0 & 0 & 0 \\ 0 & 0 & 0 & I \\ 0 & 0 & -K_m & -L \end{bmatrix}, \boldsymbol{B}_c = \begin{bmatrix} 0 \\ I \\ 0 \\ -I \end{bmatrix}$$

We also assume that sampling rate is small so that the exponential matrix $e^{A_a \Delta t}$ can be approximated by the first order Taylor expansion $e^{A_a \Delta t} \approx I + \boldsymbol{A}_a \Delta t$. After discretizing equation (31), we obtain

$$\begin{aligned} \boldsymbol{x}_a(k+1) &= \boldsymbol{A}_b \boldsymbol{x}(k) + \boldsymbol{A}_{cu} \boldsymbol{x}_a(k) + \boldsymbol{B}_b H[W_m^T(k)\widetilde{\theta}(k)] \\ \widetilde{\theta}(k+1) &= \widetilde{\theta}(k) - \Delta t \Gamma W_m(k) \gamma \ [\dot{e}_p(k) + \dot{\widetilde{q}}_p(k)] \end{aligned} \tag{32}$$

where

$$\boldsymbol{A}_b = \exp\left(\boldsymbol{A}_{\tilde{a}} \Delta t\right), \boldsymbol{B}_b = \int_0^{\Delta t} \exp\left(\boldsymbol{A}_{\tilde{a}} (\Delta t - s)\right) \boldsymbol{B}_c \, ds$$

$$\boldsymbol{A}_{\tilde{a}} = \begin{bmatrix} 0 & I & 0 & 0 \\ -K_m & -\gamma & 0 & -\gamma \\ 0 & 0 & 0 & I \\ 0 & \gamma & -K_m & \gamma - L \end{bmatrix}$$

Using the discrete time version of averaging technique [10], the average dynamics of the parameter estimation error equation in equation (32) is given by

$$\widetilde{\theta}_{av}(k+1) = \left(I - \Delta t \Gamma \ AVG\left\{W_m(k) \hat{M}_d(W_m^T(k))\right\}\right) \widetilde{\theta}_{av}(k) \tag{33}$$

where $\hat{M}_d$ is the transfer function matrix,

$$\hat{M}_d(z) = \boldsymbol{C}_b (zI - \boldsymbol{A}_b)^{-1} \boldsymbol{B}_b,\ \boldsymbol{C}_b = [0 \quad \gamma \quad 0 \quad \gamma] \tag{34}$$

and z is the Z-transform variable. Equation (33) is the sampled and zero-order hold input version of the continuous time result obtained in [8]. Therefore, $\hat{M}_d$ in equation (34) is given by

$$\hat{M}_d(z) = (1 - z^{-1}) Z\left(L^{-1}\left(\frac{1 - e^{-s\Delta t}}{s} \hat{M}_o(s) \right) \right) \tag{35}$$

where L^{-1} and Z respectively denote the inverse Laplace and Z-transforms, and $\hat{M}_o(s)$ is given in [8] as $\hat{M}_o(s) = diag\{\hat{M}_{o1}(s), \hat{M}_{o2}(s)\}$, where

$$\hat{M}_{o1}(s) = \frac{\gamma_1 L_1 s^2}{s^4 + L_1 s^3 + (2\omega_1^2 + \gamma_1 L_1) s^2 + \omega_1^2 L_1 s + \omega_1^4}$$

$$\hat{M}_{o2}(s) = \frac{\gamma_2 L_2 s^2}{s^4 + L_2 s^3 + (2\omega_2^2 + \gamma_2 L_2) s^2 + \omega_2^2 L_2 s + \omega_2^4}$$

Since the sampling frequency ($2\pi / \Delta t$) is larger than the reference resonant frequencies ω_1 and ω_2, the filtered steady state response through $\hat{M}_d(W_m^T)$ is given by

$$\hat{M}_d(W_m^T) = \begin{bmatrix} X_0 \sin(\omega_1 k) & 0 \\ A_1 Y_0 \sin(\omega_2 k + \phi_1) & A_2 X_0 \sin(\omega_1 k + \phi_2) \\ 0 & Y_0 \sin(\omega_2 k) \\ X_0 \omega_1 \cos(\omega_1 k) & 0 \\ A_1 Y_0 \omega_2 \cos(\omega_2 k + \phi_1) & A_2 X_0 \omega_1 \cos(\omega_1 k + \phi_2) \\ 0 & Y_0 \omega_2 \cos(\omega_2 k) \\ -2 A_1 Y_0 \omega_2 \cos(\omega_2 k + \phi_1) & 2 A_2 X_0 \omega_1 \cos(\omega_1 k + \phi_2) \end{bmatrix}^T \tag{36}$$

where

$$A_1 = \frac{\gamma_1 L_1 \omega_2}{\sqrt{\left(\gamma_1 L_1 \omega_2^2 - (\omega_1^2 - \omega_2^2)^2\right)^2 + L_1^2 \omega_2^2 ((\omega_1^2 - \omega_2^2)^2}}$$

$$\phi_1 = \tan^{-1} \frac{L_1 \omega_2 (\omega_1^2 - \omega_2^2)}{\gamma_1 L_1 \omega_2^2 - (\omega_1^2 - \omega_2^2)^2}$$

$$A_2 = \frac{\gamma_2 L_2 \omega_1}{\sqrt{\left(\gamma_2 L_2 \omega_1^2 - (\omega_1^2 - \omega_2^2)^2\right)^2 + L_2^2 \omega_1^2 ((\omega_1^2 - \omega_2^2)^2}}$$

$$\phi_2 = \tan^{-1} \frac{-L_2 \omega_1 (\omega_1^2 - \omega_2^2)}{\gamma_2 L_2 \omega_1^2 - (\omega_1^2 - \omega_2^2)^2}$$

Note that equation (36) has the same form as its continuous time counterpart equation in [8]. Therefore, every convergence property mentioned in the continuous time case is preserved here. Applying the decoupling condition $X_0 \omega_1 = Y_0 \omega_2$, the bandwidth of the adaptive controlled gyroscope is approximately given by

$$\tilde{\Omega}_{zav}(k+1) \approx (1 - 2\Delta t \gamma_\Omega X_0^2 \omega_1^2)\ \tilde{\Omega}_{zav}(k) \tag{37}$$

or

$$\dot{\tilde{\Omega}}_{zav} \approx -2\gamma_\Omega X_0^2 \omega_1^2 \tilde{\Omega}_{zav}$$

since the parameter estimation dynamics is much slower than the sampling rate.

This is exactly same result that was obtained for the continuous time observer-based adaptive control case, and the bandwidth of the adaptive controlled gyroscope is also approximately given by $BW \approx 2\gamma_\Omega X_0^2 \omega_1^2$. Thus, the bandwidth of a MEMS gyroscope under the observer-based discrete time adaptive control is also proportional to the adaptation gain γ_Ω and the energy of oscillation of the reference model.

Other statements made in [8] regarding the comparison between the analytical convergence rate of the angular rate estimate and simulation results for various resonant frequency ratios, and control and observer gains are also valid.

5.3 Resolution Analysis

The resolution analysis for this hybrid control system that will be presented in this section is very similar to those in [8]. The error expectation propagation of equation (22) is given by

$$\bar{\boldsymbol{x}}_d(k+1) = \boldsymbol{A}_d(k)\bar{\boldsymbol{x}}_d(k) + \boldsymbol{A}_{du}\bar{\boldsymbol{x}}_d(k) + \boldsymbol{C}_d(k)\theta \tag{38}$$

Notice that the expectation equation has the same form as its deterministic counterpart. Therefore, the mean trajectory under an stochastic environment is also biased because of the $\boldsymbol{C}_d(k)\theta$ term. Defining covariance as $\boldsymbol{P}_d = \overline{[(\boldsymbol{x}_d - \bar{\boldsymbol{x}}_d)(\boldsymbol{x}_d - \bar{\boldsymbol{x}}_d)^T]}$, the covariance propagation equation is given by

$$\boldsymbol{P}_d(k+1) \approx \boldsymbol{A}_d(k)\boldsymbol{P}_d(k)\boldsymbol{A}_d^T(k) + \boldsymbol{G}_d(k)\boldsymbol{S}_d\boldsymbol{G}_d^T(k) \tag{39}$$

The covariance $\boldsymbol{P_d}$ can easily be pre-computed independently of equation (38). The standard deviation of the angular rate estimate error is obtained from the covariance matrix $\boldsymbol{P_d}$ as

$$\sigma_{measurement} = \sqrt{\boldsymbol{H}\boldsymbol{P}_d\boldsymbol{H}^T} \tag{40}$$

where $\boldsymbol{H} = [0_{1\times 14}\ 1]$.

In this case, the resolution is a summation of the standard deviation of angular rate estimate error computed from (40) and the bias in the angular rate estimate. The ultimate achievable resolution can also be calculated by setting $S_p = 0$ and computing $\sigma_{masurement}$ with equation (40). As in the convergence rate analysis presented in [8], the same results regarding the effects of various design parameters such as control gains and parameter adaptation gains on the variance of the angular rate estimate error, can be stated in the discrete time case. In

summary, the resolution of the gyroscope can be adjusted independently by the angular rate adaptation gain, without affecting the other fabrication imperfection estimation dynamics.

The effect of the quantization noise $\delta q(k)$ on the velocity estimation may be explored in a similar way as the analysis used in section 5.1 to estimate the parameter estimate biases. Consider the noise terms in equation (21). If power of the $\delta q_d(k)$ is equal to the power spectral density of noise term $Ln_s(k)$, then the effect of quantization noise $\delta q_d(k)$ on the error dynamics of $e_p, \dot{e}_p, \tilde{q}_p, \tilde{q}_v$ and $\tilde{\theta}$ is approximately the same to that of the position measurement noise. Since the observer gain does not make any significant effects on the variance of the angular rate estimate error, we can neglect observer gain in the measurement noise terms. Thus,

$$\frac{\Delta^2}{12} I = S_p / \Delta t$$

or

$$\Delta = \sqrt{12 S_p / \Delta t} \tag{41}$$

where Δ is the quantization level.

Figure 3 shows the effect of different values of the observer gain L in predicting the effect of quantization noise. As mentioned, the effect of the observer gain is not significant. Since the quantization level is defined by the number of bits in the A/D converter as

$$\Delta = \frac{Range}{2^{Bit}} \tag{42}$$

where *Range* is a signal range to be quantized, which in this case corresponds to the velocity estimation range. From equations (41) and (42), the required A/D bit numbers for achieving the same power as the position sensing noise is

$$Bit = \log_2(Range) - \frac{1}{2}\log_2(12S_p / \Delta t) \tag{43}$$

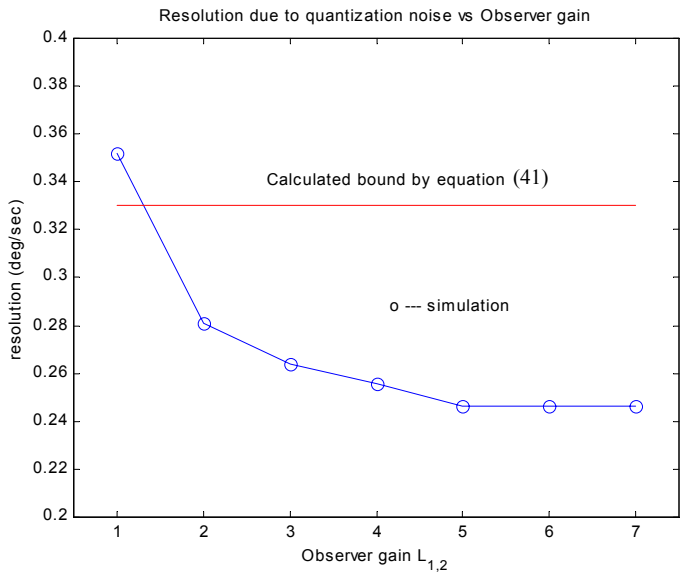

Figure 3. The effect of the observer gain in predicting
on the effect of a quantization noise

Equation (43) is a useful criterion for choosing the approximate bits numbers in an A/D converter for the velocity estimation signal. For typical numbers of the designed gyroscope, this corresponds about 16 bits. Overall, gyroscope resolution can be estimated by following formula:

$$resolution = bias + \sqrt{\sigma^2_{measurement} + \sigma^2_{quatization}} \tag{44}$$

where *bias* is a bias in angular rate estimate, $\sigma^2_{measurement}$ is a variance of the angular rate estimate error due to measurement noise, and $\sigma^2_{quantization}$ is a variance of the angular rate estimate error due to a quantization noise.

6. Simulation

A computer simulation study was conducted using the preliminary design data of the MIT-SOI MEMS gyroscope, to test the analytical results presented in this report and verify its predicted performance. The data of some of the gyroscope parameters is given by Table 1 and is same as that used in [8]. The estimate of the angular rate response to the step input angular rate is shown in Figure 4. In this figure, the upper and lower bounds, which corresponds to the analytically estimated standard deviation calculated by equation (44) are also plotted. Figure 5 shows the estimate of angular rate response to the sinusoidal input angular rate. These simulation results support the theoretical results obtained in the previous section, regarding predicted gyroscope bandwidth and resolution.

parameter	*value*
mass	5.095×10^{-7} kg
x-*axis frequency*	*4.17* KHz
y-*axis frequency*	*5.11* KHz
Quality factor	10^4
Brownian noise PSD	1.47×10^{-26} N^2sec
Position noise PSD	1.49×10^{-27} m^2sec
Velocity noise PSD	2.94×10^{-12} $(m/sec)^2$sec

Table 1. Key parameters of the designed gyroscope

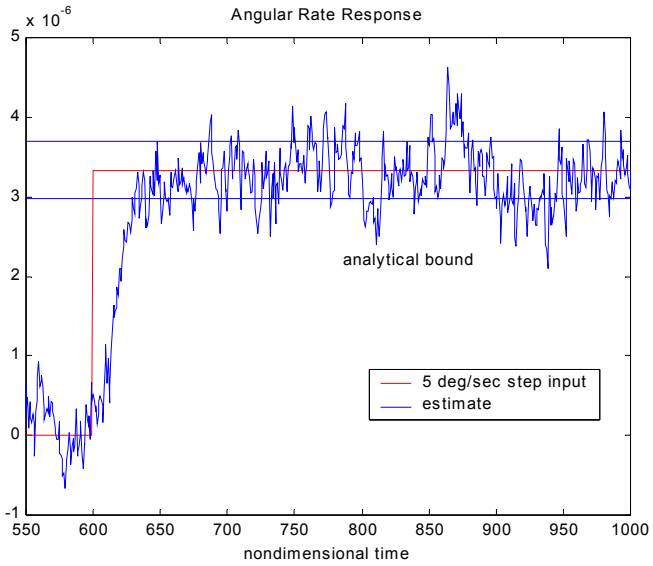

Figure 4. Time responses of angular rate estimate to the 5 deg/sec step input

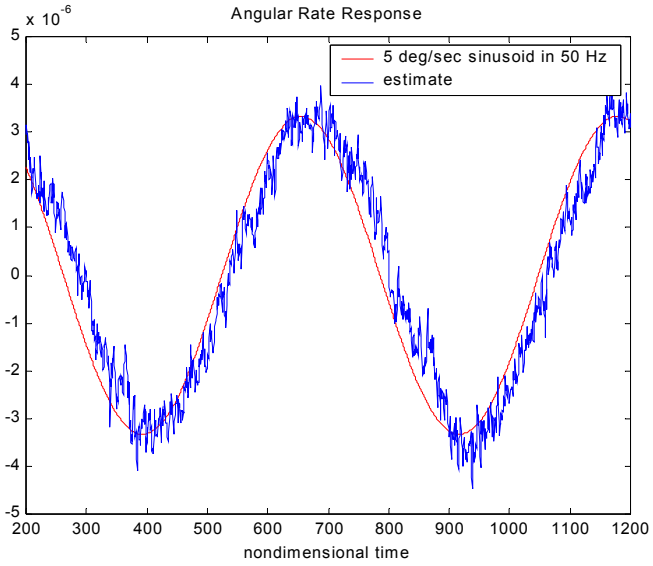

Figure 5. Time responses of angular rate estimate to the 5 deg/sec sinusoid input at 50 Hz

7. Conclusions

In this report, a discrete time version of the observer-based adaptive control system described in [8], was developed and its stability proven. This control can be readily implemented using digital processors. A stochastic analysis of this algorithm was also developed and it showed that the estimates of the angular rate and the fabrication imperfections are biased due to the signal discretization errors in the feedforward control path introduced by the sampler and holder. Thus, a two-rate discrete time control was proposed as a compromise between the measurement biases due to discretization errors and the computational burden imposed on the controller due to a fast sampling rate. In this control scheme, the parameter adaptation algorithm is updated at a slower rate than the reference signal which is used in the feedforward control. The convergence analysis of this algorithm was conducted and an analysis method was developed for determining the trade-off between the controller sampling frequency and the magnitude of the angular rate estimate biased errors. All convergence and stochastic properties of a continuous time adaptive control were preserved, and this analysis was verified with computer simulations.

References

[1] Yazdi, N., F. Ayazi and K. Najafi, "Micromachined Inertial Sensors", *Proceedings of the IEEE*, Vol.86, No.8, pp.1640-1659, Aug. 1998.

[2] Shkel, A., R.T. Howe and R. Horowitz, "Modeling and simulation of micromachined gyroscopes in the presence of imperfection", *Int. Conf. On Modelling and Simulation of Microsystems,* pp. 605-608, Puerto Rico, U.S.A., 1999.

[3] Clark, W.A., *Micromachined Vibratory Rate Gyroscopes*, Doctoral Thesis, U.C. Berkeley, 1997.

[4] Juneau, T.N, *Micromachined Dual Input Axis Rate Gyroscope*, Doctoral Thesis, U.C. Berkeley, 1997.

[5] Loveday, P.W and C.A. Rogers, "Modification of Piezoelectric Vibratory Gyroscope Resonator Parameters by Feedback Control", *IEEE Transactions on Ultrasonics,*

Ferroelectrics and Frequency Control, Vol.45, No.5, pp.1211-1215, Sep. 1998.

[6] Ljung, P.B., *Micromachined Gyroscope with Integrated Electronics*, Doctoral Thesis, U.C. Berkeley, 1997.

[7] Jiang, X., J. Seeger, M. Kraft and B.E. Boser, "A monolithic surface micromachined Z-axis gyroscope with digital output", *2000 Symposium on VLSI Circuits*, Honolulu, HI, USA, pp.16-19, June 2000.

[8] Park, S., *Adaptive Control Strategies for MEMS Gyroscopes*, Doctoral Thesis, U.C. Berkeley, 2000.

[9] Shkel, A.M., R. Horowitz, A.A. Seshia, S. Park and R.T. Howe, "Dynamics and Control of Micromachined Gyroscopes", *Proceedings of the American Control Conference*, pp.2119-2124, Jun. 1999.

[10] Bai, E-W., L-C Fu and S.S. Sastry, "Averaging Analysis for Discrete Time and Sampled Data Adaptive Systems", *IEEE Transactions on Circuits and Systems*, Vol.35, No.2, pp.137-148, Feb. 1988.

[11] Morando, A. R. Horowitz and N. Sadegh, "Digital Implementation of Adaptive Algorithms for Robot Manipulators", *IEEE International Conference on Robotics and Automation*, pp.1656-1662, May 1989.

[12] Park, S. and R. Horowitz, "Adaptive Control of MEMS Gyroscopes", *The 7th Mechatronics Forum International Conference*, Atlanta, GA, USA, Sept. 2000.

[13] Parameswaran, L., C. Hsu and M.A. Schmidt, "A Merged MEMS-CMOS Process using Silicon Wafer Bonding", *IEEE International Electron Devices Meeting*, Washington DC, pp. 613-616, Dec. 1995.

[14] Lawrence, A., *Modern Inertial Technology: Navigation, Guidance and Control*, Springer Verlag, 1993.